SCIENCE CHINA
Information Sciences

• RESEARCH PAPER •
Special Issue

August 2012 Vol. 55 No. 8: 1838–1851
doi: 10.1007/s11432-012-4625-4

Efficient DPCA SAR imaging with fast iterative spectrum reconstruction method

FANG Jian[1], ZENG JinShan[1], XU ZongBen[1]* & ZHAO Yao[2]

[1]*Ministry of Education Key Lab for Intelligent Networks and Network Security Xi'an Jiaotong University, Xi'an* 710049*, China;*
[2]*National Key Laboratory of Science and Technology on Microwave Imaging & Institute of Electronics, Chinese Academy of Sciences, Beijing* 100049*, China*

Received December 15, 2011; accepted April 25, 2012

Abstract The displaced phase center antenna (DPCA) technique is an effective strategy to achieve wide-swath synthetic aperture radar (SAR) imaging with high azimuth resolution. However, traditionally, it requires strict limitation of the pulse repetition frequency (PRF) to avoid non-uniform sampling. Otherwise, any deviation could bring serious ambiguity if the data are directly processed using a matched filter. To break this limitation, a recently proposed spectrum reconstruction method is capable of recovering the true spectrum from the non-uniform samples. However, the performance is sensitive to the selection of the PRF. Sparse regularization based imaging may provide a way to overcome this sensitivity. The existing time-domain method, however, requires a large-scale observation matrix to be built, which brings a high computational cost. In this paper, we propose a frequency domain method, called the iterative spectrum reconstruction method, through integration of the sparse regularization technique with spectrum analysis of the DPCA signal. By approximately expressing the observation in the frequency domain, which is realized via a series of decoupled linear operations, the method performs SAR imaging which is then not directly based on the observation matrix, which reduces the computational cost from $O(N^2)$ to $O(N \log N)$ (where N is the number of range cells), and is therefore more efficient than the time domain method. The sparse regularization scheme, realized via a fast thresholding iteration, has been adopted in this method, which brings the robustness of the imaging process to the PRF selection. We provide a series of simulations and ground based experiments to demonstrate the high efficiency and robustness of the method. The simulations show that the new method is almost as fast as the traditional mono-channel algorithm, and works well almost independently of the PRF selection. Consequently, the suggested method can be accepted as a practical and efficient wide-swath SAR imaging technique.

Keywords displaced phase center antenna, sparse regularization, iterative thresholding, spectrum reconstruction

Citation Fang J, Zeng J S, Xu Z B, et al. Efficient DPCA SAR imaging with fast iterative spectrum reconstruction method. Sci China Inf Sci, 2012, 55: 1838–1851, doi: 10.1007/s11432-012-4625-4

1 Introduction

Synthetic aperture radar (SAR) is a high-resolution active remote sensing system which is widely applied in many fields, including mapping, surveillance and detection. In these applications, wide ground coverage is always required for efficient use of the resources. However, to achieve a wider swath, a larger pulse

*Corresponding author (email: zbxu@mail.xjtu.edu.cn)

interval, or, equivalently, a lower pulse repetition frequency (PRF) is required to receive the long time-duration echoes, which in turn requires a lower Doppler bandwidth [1]. The contradiction between the high azimuth resolution and the wide swath is a long-standing problem in SAR system design. Some classical operation modes have therefore been developed with different emphases on the trade-off. These include the spotlight mode [2], which can provide high resolution but limited coverage, or the ScanSAR [3] and TOPS-SAR [4] modes, each of which can map a large swath but with a coarse resolution.

To essentially alleviate this conflict, simpler approaches were proposed which split the receiving antenna into multiple channels for recording and then combined the echoes using a specific reconstruction algorithm. In this way, additional information can be derived from the displaced phase center, and hence the conflict found in conventional SAR systems can be relaxed into a certain degree. For example, a multi-beam SAR mode uses multiple receiver (Rx) antennas with narrow beams directed at different areas of the detection region [5], yielding a higher resolution or a wider imaging width. However, when dealing with the high squint case, problems may arise. Another possible approach is the displaced phase center antenna (DPCA) [1,6], in which the antennas point in the same direction, extracting different parts of the azimuth samples. As a result, it allows reduction of the PRF or enhanced azimuth resolution. Extensions of the method like the quad-array SAR [7] and HRWS (high resolution wide swath) [8] further improve the performance and thus show the potential of digital beamforming in SAR imaging [9].

However, for DPCA, the traditional reconstruction method demands that the PRF should obey strict conditions to make sure that the combination of all of the receivers provides a uniform effective azimuth phase. However, the proper PRF is restricted by sampling, beam-forming, the data rate and several other conditions [1], which can severely affect the image quality. No crossing point exists for these two constraints in general, while any deviation of the PRF could produce non-uniform samples, resulting in high azimuth ambiguity if a matched filter is used directly.

On the other hand, the difficulties with DPCA seem to be much easier to tackle through appropriate signal processing. Several such works have been conducted in recent years [9,10]. For example, a Doppler spectrum reconstruction method was proposed in [10] which can significantly suppress the ambiguous energy. The true spectrum was computed using the inverse of the joint frequency information matrices acquired from a combination of all of the channels. However, such a reconstruction is not robust when the samples are approximately overlapped. Alternatively, a compressed sensing based DPCA SAR imaging framework was suggested in [11]. By establishing a precise time-domain observation model and solving the model with a sparse optimization technique, it can further suppress the ambiguity. When the observation matrix can not be decoupled, however, the dimensions of the linear system are too high to be applied, especially for large scale problems. Nevertheless, large scenes are exactly what wide swath SAR systems try to cope with.

In this paper, we propose a frequency domain method, called the iterative spectrum reconstruction (ISR) method, through integration of the sparse modeling approach and the spectrum analysis in DPCA. Without using the time-domain observation matrix, the proposed method follows the spectrum analysis of the DPCA system in [10], which is extended by importing the range cell migration (RCM), which then yields an approximated observation of the DPCA SAR system, realized via a series of decoupled linear operations. The proposed method reduces the computational cost from $O(N^2)$ to $O(N \log N)$ (where N is the total number of resolution cells), when compared with the time domain method. An acceleration strategy is also adopted to speed up the implementation of the method, based on the ability to split the observation operators into common parts and private parts. Also, the L_1 sparse regularization scheme is used, which effectively avoids the requirement for calculation of the inverse of the joint matrices while naturally cracking the RCM and retrieving the spectrum alternately during the iterations. This leads to high robustness for the algorithm. We provide a series of simulations and ground based experiments to evaluate the proposed method. The experiments demonstrate that a significant improvement can be made in the efficiency, compared to the time domain method, and in the robustness to the PRF selection, compared to the traditional spectrum reconstruction method. Consequently, the suggested method can be accepted as a practical and efficient wide-swath SAR imaging technique.

The remainder of the paper is organized as follows: In Section 2, we provide a background introduction

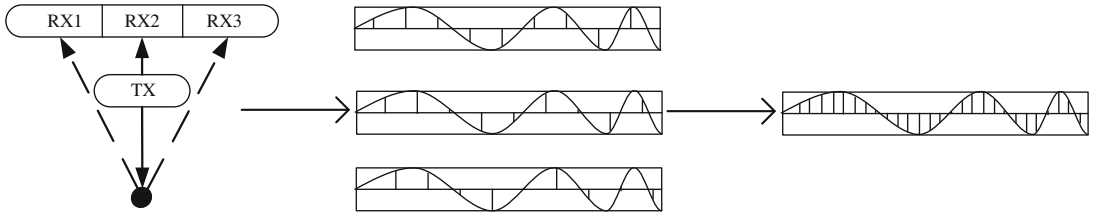

Figure 1 Illustration of DPCA SAR data accusation system.

to DPCA systems and sparse modeling, showing in particular how sparsity can be effectively applied to DPCA. The new frequency domain DPCA SAR imaging model based on sparse regularization is presented in Section 3. In Section 4, we develop a fast algorithm for solution of this model. In Section 5, we provide experimental results to demonstrate the efficiency and robustness of the proposed method. Finally, we provide concluding remarks in Section 6.

We use the following notations throughout the paper: column vectors and matrices, and operators are denoted by bold lower case, $\boldsymbol{x}$, bold upper case, $\boldsymbol{A}$, and Roman upper case, C, respectively. $\boldsymbol{A}^{\mathrm{T}}$, $\boldsymbol{A}^{*}$ and $\boldsymbol{A}^{\mathrm{H}}$ denote the transpose, conjugate and Hermitian transpose of $\boldsymbol{A}$, respectively.

2 DPCA and sparse modeling

In this section, some necessary knowledge on DPCA and sparse modeling is provided. In particular, we introduce a general two-dimensional (2D) model of the DPCA SAR linear system in an accurate form, and we then present a general account of the compressed sensing and regularization approach.

2.1 DPCA SAR signal model

As shown in Figure 1, in a DPCA SAR system, a signal is transmitted by a single transmitter while the backscattered energy is received by multiple receiving antennas, resulting in a sequence of received echoes with displaced time delays. The delay signature is given by the relative distance from each receiving antenna to the transmitting antenna, i.e., $\Delta x_i = x_i - x_0, i = 1, 2, \ldots, n$, where n is the number of sub-receivers. The received echo from the receiving channel i can be described as [12]

$$s(\eta', \tau') = \int\int f(\eta, \tau) g_i(\eta' - \eta, \tau'; \tau) \mathrm{d}\eta \mathrm{d}\tau + n_i(\eta', \tau'), \tag{1}$$

where

$$g_i(\eta' - \eta, \tau'; \tau) = \omega_\eta^{(i)}(\eta' - \eta)\omega_\tau\Big(\tau' - \frac{2R_i}{\mathrm{c}}\Big) \exp\left[-\frac{4\pi R_i}{\lambda} + \phi\Big(\tau' - \frac{2R_i}{\mathrm{c}}\Big)\right], \tag{2}$$

λ is the carrier wavelength, c is the velocity of light, v is the velocity of the platform, ω is the envelope function, f is the scene reflectivity, η and τ are the slow time (azimuth) and the fast time (range), respectively, n_i is the additional white noise, and ϕ is the transmitted pulse. We see from (1) and (2) that the slant ranges of the different channels are different, and are defined by

$$R_i(\eta' - \eta; \tau) = \frac{1}{2}(\sqrt{(\tau \mathrm{c}/2)^2 + [v(\eta' - \eta)]^2} + \sqrt{(\tau \mathrm{c}/2)^2 + [v(\eta' - \eta) - \Delta x_i]^2}), \tag{3}$$

where the second term determined by Δx_i is the main difference.

According to the mechanism of SAR, the acquisition of the azimuth signal is equivalent to sampling of the continuous azimuth signal using the PRF. However, the PRF is always constrained by several factors in a DPCA setting [1]. First, the PRF should provide an adequate azimuth bandwidth. In DPCA, the bandwidth is acquired from a combination of sub-apertures and thus the PRF can take fewer samples than that required by the Nyquist criterion, which yields a relaxation of the contradiction of high resolution and wide-swath, resulting in the expected larger swath. Second, to avoid nadir returns and to minimize the

ambiguity level caused by the antenna pattern, a timing diagram is always needed to guide the selection of the PRF. The selection of the PRF is also constrained by the DPCA system, which assumes that the SAR platform moves by just one half of its total antenna length between subsequent radar pulse, as it is known that PRF equals to $\frac{2v}{n\Delta x}$, where Δx is the interval between the sub-apertures. In this way, a simple arrangement of the samples from the sub-apertures will result in uniform sampling of the azimuth signal, as shown in Figure 1, and it can then be focused using algorithms designed for mono-channel SAR, such as the range Doppler algorithm (RDA). Nevertheless, such a PRF selection may not fall in the valid area of the timing diagram, and therefore may not always obey the DPCA constraint. As a result, the deviation of the PRF leads to an incorrect focus if we use a matched filter. As the problems caused by the nadir returns and the antenna pattern are more difficult to resolve, an unambiguous image reconstruction technique for the non-uniform case is required. In [10], the author provided a novel technique which can unify the ambiguous information of the sub-apertures to reconstruct the unambiguous spectra. However, the method does not work well when the samples approach each other. In this paper, our aim is to develop a more efficient method through combination of the benefits of spectrum analysis in DPCA and sparse modeling in compressed sensing (CS). To this end, we extend the CS based SAR imaging model in [11] into a 2D case.

2.2 DPCA with sparse regularization

Sparse modeling aims to find solutions for a linear system with as few nonzeros entries as possible [13]. The CS paradigm has been applied to recover a signal from measurements below the Nyquist rate. When applied to SAR imaging, it is known that with appropriate regularization schemes (e.g. L_q regularization with $0 < q \leqslant 1$), a higher resolution and lower sidelobe image can be reconstructed from very few samples, and from far less than the number required by the Nyquist rate.

To apply the sparse modeling approach to DPCA SAR systems, we must first specify the observation model, which can be obtained as follows. The scene reflectivity $f(\eta, \tau)$ is first sampled with the frequency of the PRF along the azimuth and the rate of the analog-digital converter along the range, resulting in the 2D arrays $\boldsymbol{X}, \boldsymbol{Y}_i$. The two arrays are then vectorized into $\boldsymbol{x}$ and $\boldsymbol{y}_i$ while the discretionary weight derived from (1) is simply the observation matrix $\boldsymbol{H}_i$, leading to $\boldsymbol{y}_i = \boldsymbol{H}_i\boldsymbol{x}$, where $\boldsymbol{H}_i \in C^{\frac{N}{n}\times N}, \boldsymbol{y} \in C^{N\times 1}$ and $i = 1, 2, \ldots, n$. We then combine all of the measurements from the sub-receivers, which reduces to $\boldsymbol{H} = [\boldsymbol{H}_1, \boldsymbol{H}_2, \ldots, \boldsymbol{H}_n]$, and $\boldsymbol{y} = [\boldsymbol{y}_1^{\mathrm{T}}, \boldsymbol{y}_2^{\mathrm{T}}, \ldots, \boldsymbol{y}_n^{\mathrm{T}}]^{\mathrm{T}}$. Therefore, the overall echoes from all the channels can be naturally modeled as a linear function of the backscattered reflectivity:

$$\boldsymbol{y} = \boldsymbol{H}\boldsymbol{x} + \boldsymbol{n}_0, \tag{4}$$

where $\boldsymbol{n}_0$ is the noise. To solve the above model, the least squares(LS) method is normally adopted whenever the measurements are taken according to the Nyquist criterion (in this case, the $\boldsymbol{y}$ dimension is larger than the $\boldsymbol{x}$ dimension). However, when we attempt to reduce the number of measurements required (i.e., by sampling at less than the Nyquist rate), the LS method does not work well. In this case, the regularization approach is then a suitable alternative choice.

Furthermore, a sparse regularization method would be a more satisfying alternative whenever the observed scene is compressible or sparse. The sparse regularization method is also feasible because it can not only relax the demand for measurements, but can also improve the image quality [14].

A sparse regularization method for the solution of (4) can generally be modeled as

$$\min_{\boldsymbol{x}} \ \{\|\boldsymbol{y} - \boldsymbol{H}\boldsymbol{x}\|_2^2 + \lambda\rho(\boldsymbol{x})\}, \tag{5}$$

where $\rho(\boldsymbol{x})$ is the sparsity constraint, and λ is the regularization parameter. The function of $\rho(\boldsymbol{x})$ is to regularize the behavior of the solution $\boldsymbol{x}$ to avoid overfitting or unwanted artifacts. Following the approach of [15], we only consider the case where

$$\rho(\boldsymbol{x}) = \|\boldsymbol{x}\|_q^q = \sum |\boldsymbol{x}_i|^q, \tag{6}$$

where $q \in [0, 1]$ is a positive real number. As such, (6) is referred to as L_q regularization.

When q is specially chosen, say, $q = 0, \frac{1}{2}, \frac{2}{3}, 1$, a very fast iteration method, called the iterative thresholding algorithm (ITA) [16], exists, which is defined as

$$\boldsymbol{x}^{(j+1)} = E_{q,\lambda\mu}(\boldsymbol{x}^{(j)} + \mu \boldsymbol{H}^{\mathrm{T}}(\boldsymbol{y} - \boldsymbol{H}\boldsymbol{x}^{(j)})), \tag{7}$$

where $E_{q,\sigma}$ is a so-called thresholding operator and μ is a normalized parameter. The operator $E_{q,\sigma}$ is diagonally nonlinear, i.e., it can be expressed in the form

$$E_{q,\sigma}(\boldsymbol{x}) = [e_{q,\sigma}(\boldsymbol{x}_1), e_{q,\sigma}(\boldsymbol{x}_2), \ldots, e_{q,\sigma}(\boldsymbol{x}_N)]^{\mathrm{T}} \tag{8}$$

with a specific thresholding function $e_{q,\sigma}(\boldsymbol{x}_i)$, the convergence of ITA for $q = 1, \frac{1}{2}$ has been verified in [15] and [16] .

Based on the use of L_q regularization with ITA, several sparse SAR imaging methods have been suggested in recent years [17][1)]. All of these applications support the effectiveness and promise of such new types of SAR imaging technology. The challenge is, however, the high computational cost required for the solution of (4) when the observation matrix is calculated. This challenge will increase further if the model in (5) is used directly for DPCA SAR imaging, because the scale of the wide swath problem is always very large and the matrix computation of $\boldsymbol{H}$ is very time-consuming.

3 DPCA Observation model with frequency domain methods

In SAR signal processing, although the data are acquired in the time domain, frequency domain based matched filtering (MF) methods are always used to reconstruct the image [12]. This type of algorithm is extremely efficient, because of their fast implementation of the fast Fourier transformation (FFT). We therefore anticipate finding a frequency domain based method to deal with the DPCA SAR imaging problem and implement (7) more efficiently. In this section, we introduce a new reconstruction method that combines sparse modeling with spectrum analysis of DPCA SAR signal.

The main idea is to approximate the observation matrix $\boldsymbol{H}$ in (5) by using a sequence of frequency domain operators, which can be implemented quickly as the MF. To this end, we follow some of the work of [10] and introduce a frequency domain observation model of the DPCA SAR signal.

3.1 Spectrum analysis of DPCA signal

In DPCA, the multiple receivers share a similar operating mode so that they can always be analyzed in the same way. In general, the analysis of the DPCA signal can be commonly decomposed into three parts, the azimuth modulation, the range cell migration and the spectrum folding.

For the azimuth modulation, the azimuth response of a single target in channel i can be described by a filter $h_i(f)$ shown in the second exponential term in (2). As in [12], according to Taylor expansion and the principle of stationary phase (POSP), $h_i(f)$ can be approximated in the Doppler domain as follows:

$$h_i(f; R_0) = c_i \exp\Big[-j\frac{\pi \Delta x_i^2}{2\lambda R_0}\Big] \exp\Big[-j\frac{\pi \Delta x_i}{v} f\Big] \exp\Big[j\frac{\lambda R_0}{2v^2} f^2\Big], \tag{9}$$

where f is the Doppler frequency. The azimuth filter h_i mainly consists of three phase terms. The first term is a constant phase, the second exponential term is a linear phase representing the time delay derived from the relative distance between the receiving and transmitting antennas, and the third exponential term is a quadratic phase which is the same as the mono-channel azimuth filter. The most prominent difference between the individual channels is the time shift $\frac{\Delta x}{2v}$, which is then used to synthesize a higher bandwidth signal, to achieve the goal of wide swath imaging.

The range cell migration caused by the change in the slant range along the flight path, according to [12], can be approximated commonly using the following interpolation procedure

$$\tilde{h}_i(\tilde{f}, \tilde{\tau}) = \sum_{\tau} h_i(f, \tau) \mathrm{sinc}(\tilde{\tau} - (\tau + \Delta R(f, \tau))), \tag{10}$$

1) Fang J, Xu Z B, Zhang B C, et al. Fast compressed sensing SAR imaging based on approximated observations. Submitted to IEEE Transactions on Geoscience and remote sensing

where τ denotes the range cells, $\Delta R(f) = \frac{\lambda^2 R_0 f^2}{8v^2}$ is the amount of RCM, and $\tilde{h}_i$ is the signal h_i after range cell migration. From (10), one can see that the amount of RCM is nearly the same for each channel, because all of the receiver channels share the same Doppler center. The unified RCM makes the cracking process much more efficient, and thus, ensures the practical use of the DPCA.

The spectrum folding is unique for the multiple-channel DPCA setting, as compared with that for the mono-channel SAR case. Because the azimuth sampling rate PRF is lower than that required by the Nyquist rate, the data in each receiver in a DPCA setting are always under-sampled. To analyze the effects of undersampling, we assume a maximum processed Doppler bandwidth of $n\cdot$ PRF (consider n channels). Then, after sampling at the PRF, a spectrum with a frequency larger than the PRF will be folded into the baseband $[-\frac{\mathrm{PRF}}{2}, \frac{\mathrm{PRF}}{2}]$, which can be described by

$$\hat{h}_i(f,\tau) = \sum_{k=-n/2}^{n/2} \tilde{h}_i(f + k\cdot \mathrm{PRF}, \tau). \tag{11}$$

The final acquired azimuth filter $\hat{h}$ can approximate the azimuth response of the target well, making full use of the unique features of DPCA SAR observation. It should be noted that we neglect to discuss the range modulation of this approach here, because it is the same as that for the traditional mono-channel model. Also, the raw data can be preprocessed for range compression to avoid additional computational costs.

3.2 Sparse regularization model

The spectrum analysis above has built a relationship between the reflectivity of the scene and the raw data, which is realized via the azimuth filter $\hat{h}_i(f,\tau)$. To use it in the regularization problem (5), we explicitly describe the operator form of this relationship as follows:

$$\hat{\boldsymbol{Y}}_i = G_i(\boldsymbol{X}) = \boldsymbol{S}D(\boldsymbol{P}_i \odot \boldsymbol{F}\boldsymbol{X}), \tag{12}$$

where $\boldsymbol{X}$ and $\hat{\boldsymbol{Y}}_i$ represent the SAR image and the raw data in the ith channel after preprocessing respectively, $\boldsymbol{F}$ is the matrix for the Fourier transition along the azimuth, $\boldsymbol{P}_i$ is the phase matrix acquired by (9), $\odot$ is the Hadamard product for element-wise multiplication, D is a sinc-kernel interpolation operator from (10) with a kernel length n_k, and $\boldsymbol{S}$ is the matrix for the spectrum folding which can be implemented directly as the spectrum summation in (11).

As shown in (12), the observation G_i consists only of decoupled operations so that it can be efficiently computed. The linear problem of (12) is commonly solved by taking the inverse of a unified observation (combining all channels), as in [10]. However, the method is sensitive both to the interval of the receiving antennas and to the errors in RCM correction (RCMC). Alternatively, we use the sparse regularization model, which can improve the robustness for reconstruction. By combining all of the subapertures, a regularized model can be written as

$$\sum_{i=1}^{n} \|\hat{\boldsymbol{Y}}_i - \boldsymbol{S}D(\boldsymbol{P}_i \odot \boldsymbol{F}\boldsymbol{X})\|_F^2 + \lambda \|\boldsymbol{X}\|_q^q, \tag{13}$$

where $\|\cdot\|_F$ is the Frobenius norm. The first term in (13) sums up the representation error from all receivers, yielding a PRF irrelevant approximation with fast operators. The second term is a sparse regularization which is used to suppress the sidelobe and the sensitivity at the PRF.

4 The iterative spectrum reconstruction algorithm

In this section, we introduce the iterative spectrum reconstruction algorithm for the proposed DPCA SAR imaging model. The suggested algorithm is based on the ITA in (7), but with the observation of (12) instead. The acceleration is then addressed by separating the azimuth filter into shared parts and private parts, and thus the calculation is simplified, and yields a faster algorithm.

4.1 Reconstruction framework based on iterative thresholding

As discussed in Section 2, the ITA provides a simple but effective strategy when solving a sparse optimization problem. However, performing it exactly using the observation matrix is too time-consuming. We aim to solve (13) instead by taking advantage of the fast calculation of G_i. According to the iteration scheme of the ITA in (7), the only thing needed to solve (13) is the conjugate transposition of operator G_i. Fortunately, this can be calculated separately from the suboperators in (12), to derive the ISR. We derive it in detail from four aspects. First, it is obvious that $\boldsymbol{F}^{\mathrm{H}}$ is the inverse FFT, $\boldsymbol{F}^{-1}$. Second, the conjugate transposition of phase multiplication by $\boldsymbol{P}_i$ is simply a phase multiplication by $\boldsymbol{P}_i^*$. Third, $\boldsymbol{S}^{\mathrm{T}}$ is equivalent to an operation which expands the spectra with a replicated frequency, say $h(f + k \cdot \mathrm{PRF}) = h(f), k = -n/2, \ldots, n/2$. Finally, the transposition of D can be represented by the following operator, which is the exact interpolation for RCMC[1)]:

$$h(f,\tau) = \sum_{\tilde{\tau}} \tilde{h}(\tilde{f},\tilde{\tau})\mathrm{sinc}(\tilde{\tau} - (\tau + \Delta R(f,\tau)). \tag{14}$$

According to these deduction, G_i^{H} can be expressed using

$$M_i(\boldsymbol{Y}) = \boldsymbol{F}^{-1}C(\boldsymbol{P}_i^*\boldsymbol{S}^{\mathrm{T}}\boldsymbol{Y}), \tag{15}$$

where C is the interpolation in (14). Then the iteration scheme for solving (13) is given by

$$\boldsymbol{X}^{(j+1)} = E_{q,\lambda\mu}\left\{\boldsymbol{X}^{(j)} + \mu\sum_{i=1}^{n} M_i[\widehat{\boldsymbol{Y}}_i - G_i(\boldsymbol{X}^{(j)})]\right\}. \tag{16}$$

According to the establishment of M_i, the above iteration is implemented accurately, and thus the convergence of (16) holds naturally. More importantly, all of the operations in (16) are decoupled with frequency domain operations, and thus they are very fast.

Finally, we discuss the parameters. First, the normalization parameter μ is selected to ensure the convergence of the algorithm. Although it can be searched for as the gradient step size in every loop, we prefer a value between 0.01 and 0.1 (because the azimuth filter is already normalized), which can be searched in several iterations at the beginning of the algorithm. The regularization parameter λ is set to tradeoff the abilities of data fitting and quality enhancement. To achieve a high quality image with low information loss, we recommend a strategy where $\lambda\mu$ decreases from a large value (for example, -20 dB of the largest magnitude of the current loop) to provide sufficient regularization, and then to the required smallest magnitude of the system, which ensures the successful reconstruction of inconspicuous targets.

4.2 Acceleration with filter separation

A direct implementation of the algorithm given in (16) will bring redundant computational costs. The Landweber step for each channel (inside the summation) must be calculated independently, leading to n times the computational cost when compared with the mono-channel case. However, recalling the approximation operator G and the azimuth filter (9), we find that only a small part is different for each receiver. Therefore, we divide $\boldsymbol{P}_i$ into $\boldsymbol{P}_i = \boldsymbol{Q} \cdot \boldsymbol{Q}_i$, where $Q(f; R_0) = \exp[j\frac{\lambda R_0}{2v^2}f^2]$ is the chirp azimuth filter shared by all channels and $Q_i(f, R_0) = \exp[-j\frac{\pi\Delta x_i^2}{2\lambda R_0}]\exp[-j\frac{\pi\Delta x_i}{v}f]$ is specific for individual channels. We then assuming a slight variance of the velocity between adjacent range cells, and the operations of phase multiplication by $\boldsymbol{Q}_i$ and RCMC D can be commutated, resulting in an alternative iteration:

$$\boldsymbol{X}^{(j+1)} = E_{q,\lambda\mu}\left\langle \boldsymbol{X}^{(j)} + \mu M_0\left\{\sum_{i=1}^{n}\boldsymbol{Q}_i^*\boldsymbol{S}^{\mathrm{T}}[\widehat{\boldsymbol{Y}}_i - \boldsymbol{S}\boldsymbol{Q}_i\mathrm{G}_0(\boldsymbol{X}^{(j)})]\right\}\right\rangle, \tag{17}$$

where $G_0(\boldsymbol{X}) = D(\boldsymbol{Q}\odot\boldsymbol{F}\boldsymbol{X})$, and M_0 is its conjugate transposition. The implementation of the algorithm is shown in Figure 2, which separates the whole procedure into four parts. The first simulates the shared

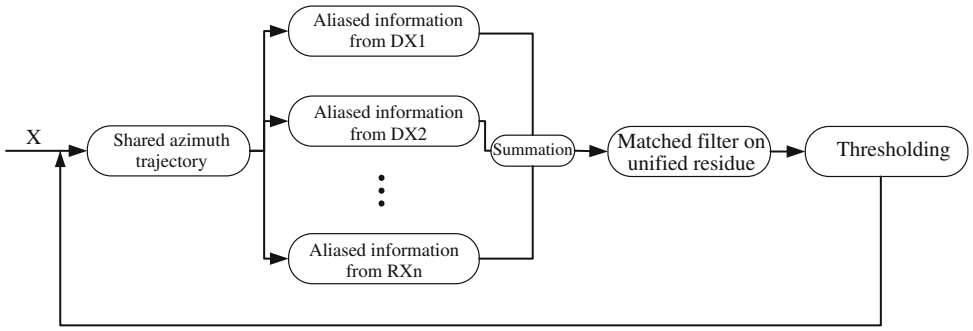

Figure 2 Block diagram of the iterative spectrum reconstruction algorithm.

Algorithm 1 The iterative spectrum reconstruction algorithm for DPCA SAR imaging

Require: Preprocessed SAR raw echoes $\boldsymbol{Y}_i, i = 1, 2, \ldots, n$, regularization parameter λ.

Ensure: The recovery image $\boldsymbol{X}^*$

Initial: $\boldsymbol{X}^{(0)} = 0$,λ, μ and max iteration $I_{\max}$

for $j = 0$ to $I_{\max}$ **do**

Standard Doppler Signal Simulation: $\boldsymbol{U}^{(j)} = \mathrm{D}(\boldsymbol{Q} \odot \boldsymbol{F}\boldsymbol{X})$

for $i = 1$ to n **do**

Residue for receiver i: $\boldsymbol{R}_i^{(j)} = \boldsymbol{Y}_i - \boldsymbol{S}\boldsymbol{P}_i\boldsymbol{U}^{(j)}$

end for

Spectrum reconstruction: $\boldsymbol{V}^{(j)} = \boldsymbol{S}^{\mathrm{T}} \sum_{i=1}^{n} \boldsymbol{Q}_i^* \boldsymbol{R}_i{}^{(j)}$

RCMC and azimuth compression: $\Delta\boldsymbol{X}^{(j)} = \boldsymbol{F}^{-1}\boldsymbol{P}^*\mathrm{C}(\boldsymbol{V}^{(j)})$

Thresholding: $\boldsymbol{X}^{(j+1)} = \mathrm{E}_{q,\lambda\mu}(\boldsymbol{X}^{(j)} + \mu\Delta\boldsymbol{X}^{(j)})$

end for

azimuth trajectory. The second is a specific procedure which includes an additional phase multiplication, a spectrum summation and their conjugate transposition. The third is a traditional matched filter procedure on the summed residue. Finally, a thresholding procedure is used to regularize the error and the noise in the current estimation of $\boldsymbol{X}$. The most costly procedures, the FFT and the interpolation, are run only once per iteration, irrespective of the number of receiver n. Also, the thresholding taken together with the circular update of $\boldsymbol{X}$ provides a profound evaluation of the reconstruction, which can ensure robust results. For convenience of use, we list pseudo-code of (17) as Algorithm 1.

In summary, the proposed algorithm can be featured as a fast iterative spectrum reconstruction method. By approximating the spectrum instead of the raw signal, frequency domain operations are available to accomplish all of the computations, and are extremely fast. Meanwhile, the iterative scheme is used to alternatively measure the approximation error and crack the range cell migration. Because of the complex arrangement of the multiple channel receivers, the range cell migration is difficult to crack in a single step. In an iterative setting, the feedback from the measurement of the reconstruction error can act as a guide to how RCMC can be correctly performed in the next iteration. Therefore, when compared with the single step algorithm of [10], the proposed method can work more effectively.

4.3 Remarks

In this section, we list the main advantages of the proposed method when compared to the time domain method. The improvements from the proposed method can be summarized into the following four aspects:

1) The suggested algorithm does not need to save the costly matrix $\boldsymbol{H}$ which has dimensions that are nearly the square of the size of the scene. Instead, some phase and parameter matrices with scales lower than the raw data are calculated. The proposed method therefore saves memory.

2) The computational complexity of the ISR in a single step is $O(N \log_2 N)$, benefiting from the frequency domain operations, and is essentially faster than the $O(N^2)$ value of the time domain method.

Table 1 Primary parameter of SAR system and geometry

Parameter	Symbol	Simulation	Ground-based
Number of subreceivers	n	3	3
Length(Interval) of subreceivers (m)	Δx	3	0.032
Slant range of scene center	R_c	10 km	2.96 m
Effective radar velocity(m/s)	V	300	1
Beam squint angle(rad)	θ	0	0
Radar center frequency(GHz)	f_0	5	17
Pulse repetition frequency(Hz)	F_a	86.67	41.67

The iteration commonly takes 30 steps, leading to at most 30 times the computation compared with traditional mono-channel method, but the performance of this iteration is much better.

3) The iteration can be implemented easily. The familiar procedures including FFT, phase multiplication and RCMC make the algorithm very simple and comprehensible.

4) The method benefited from the division of the azimuth filter, making computational complexity corresponding to the individual receiver sufficiently low, and leading to an efficient method.

Also, the proposed algorithm demonstrates that by using the sparse modeling method, PRF may not be a critical factor in the DPCA SAR system. We show that the sensitivity of the PRF can be empirically alleviated in the following simulations and applications.

5 Experiments

In this section, a series of simulations and applications are presented. Their main purpose is to examine whether the proposed method can achieve an unambiguous image with non-uniform sampling, how the PRF affects the performance of the algorithm, and whether it can work in a practical case. We designed some experiments to answer the questions.

The primary parameters of the simulations and the ground-based experiments are given in Table 1. In brief, we refer to the traditional range-Doppler algorithm as RDA, the method in [10] which aims to reconstruct the spectrum as SR, the compressed sensing based method in [11] as CSR and the proposed method to iteratively reconstruct the spectrum as ISR. We consider only noise-free cases to achieve a more detailed comparison among the different algorithms.

5.1 Simulation

We implement several simulations in this section to compare the performances of the different reconstruction algorithms. A 2D point target simulation is presented first to evaluate and validate the proposed method in DPCA SAR imaging with non-uniform cases. Then, an experiment is conducted to study the impact of the PRF on the level of ambiguity. In this experiment, the PRF is chosen in a wide range, which provides a thorough insight into the influence of the PRF on the performance of DPCA SAR imaging.

The number of sub-receivers is set to three and the raw data are generated in the time-domain using an exact slant range. The weight of the antenna is chosen with a rectangular shape which can avoid the ambiguous energy from the antenna diagram. Also, the antennas are arranged so that the uniform sampling condition is satisfied when the PRF is chosen as B_a/n (where $B_a = 200$ Hz is the Doppler bandwidth). Otherwise, any trivial deviation will cause nonuniform sampling.

1) Reconstruction ability: In this experiment, the ambiguity suppression ability is evaluated, where the ambiguity level is defined as the ratio of the maximum response in the aliased region to the amplitude of the target. We start with a 2D simulation (for RDA, only a 1D simulation is performed because the RCM is hard to crack in non-uniform cases), in which five points are located at the center with unit amplitudes and uniform phases. A chirp signal is transmitted with a bandwidth of 100 MHz and the PRF is set to be 86.67 Hz (the maximum observable Doppler bandwidth is $86.67 \times 3 = 260$, which is 1.3 times the

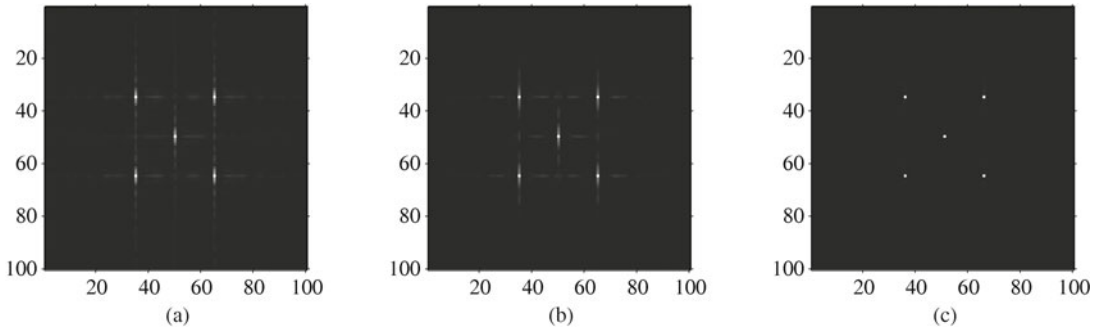

Figure 3 The reconstruction results of 5 point target simulations with different methods. (a) Reconstructed using SR; (b) reconstructed using ISR; (c) reconstructed using CSR.

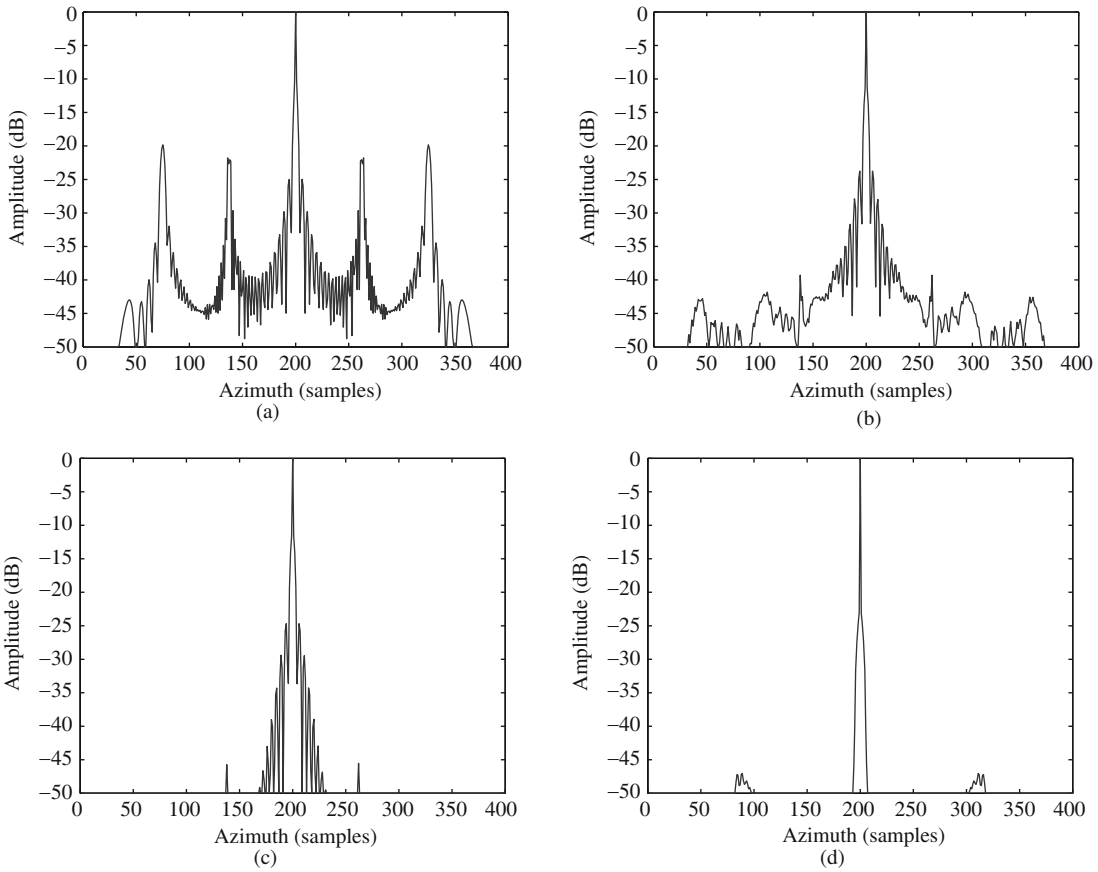

Figure 4 The azimuth slice of the center target. (a) Result from RDA; (b) result from SR; (c) result from ISR; (d) result from CSR.

assumed Doppler bandwidth), yielding a highly non-uniform case. Some of the results are shown in Figure 3.

As seen in Figure 3, SR, CSR and ISR can all reconstruct the image successfully with no obvious ambiguity. More specifically, we can also observe the levels of the sidelobes from SR to ISR are almost the same, but SR has a little ambiguity along the azimuth direction. The result for CSR shows better performance with almost no sidelobe or ambiguity.

For a more detailed analysis, we take an azimuth slice at the center of the scene where a single target is located. We add the 1D performance of RDA into the comparison. Figure 4(a) indicates that RDA performs badly in the non-uniform case. There is approximately -20 dB energy for both the first and second ambiguities (the number of the ambiguity is related to the number of the sub-receiver). With the Doppler spectrum reconstruction shown in Figure 4(b), the ambiguous energy can be reduced to -38 dB.

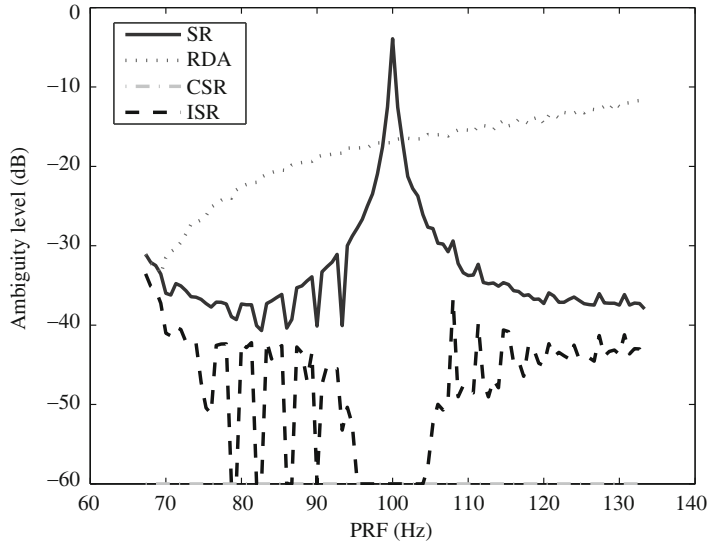

Figure 5 The impact of PRF on various algorithms.

This is effective because non-uniform, but regular samples can provide clear guidance for the reconstruction of the true spectrum. When we come to the proposed method shown in Figure 4(c), it can be seen that the ambiguous energy is further suppressed to −46 dB. This improvement is acquired by sparse regularization, which can better accumulate the energy. The time domain reconstruction method CSR based on sparse modeling achieves the best reconstruction, and can acquire a much sharper response. Because the matrix is built exactly without any errors, it has obvious advantages over the frequency domain methods, which use approximation by Taylor expansion, POSP. However, RDA, SR, ISR and CSR take 0.5, 2, 10 and 700 s (200 s to establish the observation matrix $\boldsymbol{H}$ and 500 s in the reconstruction process) for reconstruction, respectively. There is a significant increase in speed for ISR over the time domain method CSR. However, the size of the simulation is only 300×300 pixels, and the improvement would be much more obvious in a practical wide swath SAR imaging task (with dimensions of at least a million pixels).

2) Robustness on PRF: In the previous section, the validation of the proposed method was demonstrated. Next, we show how PRF affects the reconstruction process. A 1D simulation was performed with a point target located at the center. We vary the PRF and take the level of the ambiguity as an index for the reconstruction result. The relationship between the ambiguity level and the PRF will show whether the PRF is a critical constraint in DPCA SAR imaging and whether the proposed method can robustly reconstruct the image. To achieve this goal, the PRF in these experiments ranges widely, from 60 Hz to 140 Hz, which yields $B_a/n < \text{PRF} < 2B_a/n$. Because the length of the sub-aperture is just 3 m, there are cases where the phase center of the sub-receiver is highly correlated, and they even coincide when PRF$= 1.5B_a/n$. This will bring failure when attempting to solve using SR, because the inverse is not well defined. Figure 5 shows the curves for all four methods.

We can see from Figure 5 that the selection of the PRF seriously affects the RDA. With increasing PRF, the energy of the ambiguity increases rapidly, with an average level beyond −15 dB. For SR, a much better performance is produced with lower average ambiguity. It begins with the same performance as RDA, because there is no distinction when the PRF satisfies the traditional constraints of DPCA, and a small variance does not suddenly affect the performance. It works well in many cases, but when the samples approximately coincide, i.e. when the PRF is near 100 Hz, the performance degrades dramatically, which is caused by the inverse calculation using a badly scaled matrix. It is even worse than the RDA when the PRF$=$ 100 Hz (in this case, no target can actually be seen). When we come to the proposed method, we find that it is more robust, with no sudden changes, while the ambiguous energy is constantly below −35 dB, which is an average 15 dB improvement in the ability for ambiguity reduction over SR. This phenomenon arises from the fact that we calculate the 'inverse' based on a robust sparse regularization

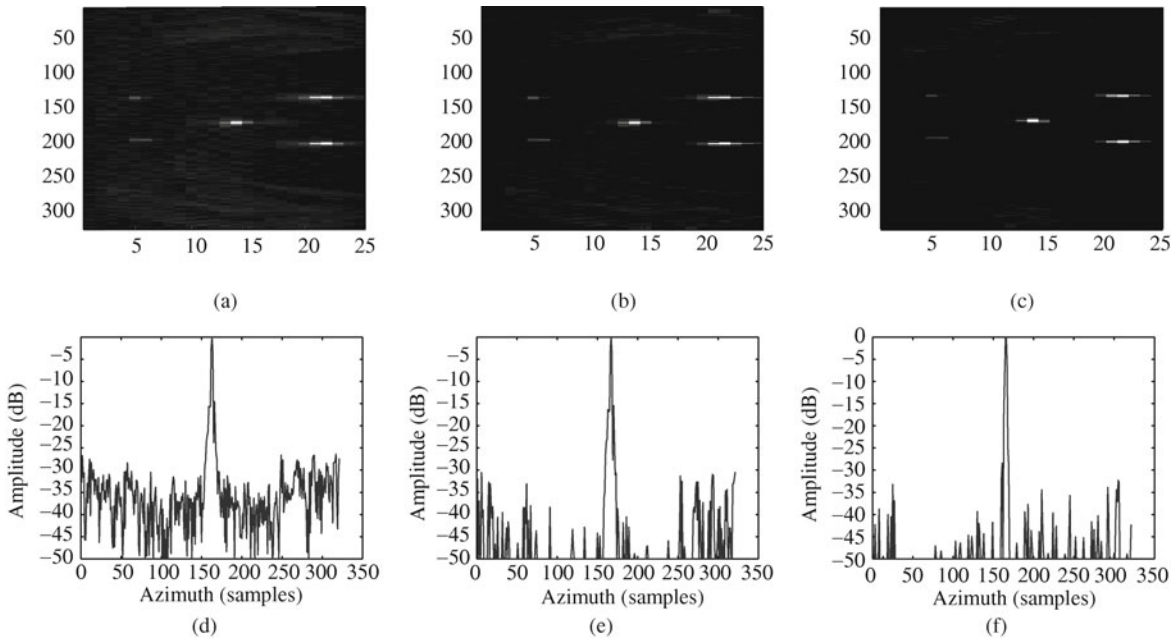

Figure 6 Reconstruction of ground-based data in uniform case. (a) 2D result of SR; (b) 2D result of ISR; (c) 2D result of CSR; (d) azimuth profile of SR; (e) azimuth profile of ISR; (f) azimuth profile of CSR.

model, the impact from the singularity can then be released. Finally, the CSR provides the least sensible results. Because it is the precise description of the DPCA model, we concluded that the PRF is not a critical factor in DPCA, which can be compensated by using the appropriate algorithms, e.g. sparse regularization. Although the approximation used in ISR is still too coarse to achieve the same result, it is much faster than the completely time domain-based methods.

5.2 Ground based experiments

In the previous section, we showed the performance of our method on simulated data. In this section, the proposed method is verified using a ground-based DPCA SAR imaging system. There is a single aperture transmitting a step frequency signal, along with three other apertures to receive the echoes. The main system parameters are given in Table 1. There are five targets at the center of the scene, which are three trihedral corner reflectors and two metal balls. The data are sampled at intervals of 0.004 m originally, but are then down-sampled (6 times) with different starting range cells (no preprocessing is included). We could therefore simulate various conditions for effective phase center combinations, which has the same effect as changing the PRF. The raw data are used to synthesize cases where the effective antenna intervals are 0.032, 0.040, and 0.024 m, which are the uniform case, the highly non-uniform case and the overlapping case, respectively. Also, to eliminate the intrinsic phase differences from different receiving hardware, the raw data are normalized (in terms of phase and magnitude) according to the center target. Some of the results obtained are shown in Figures 6 and 7.

When we come to the uniform case shown in Figure 6, we see successful reconstruction using all four methods (RDA is the same as SR). However, ISR and CSR provide much clearer results than SR, while the sidelobe of CSR is the lowest. We then take the slice of the center target shown in the second row. The main ambiguous energy of SR is about -25 dB. When incorporating sparse regularization, the ambiguity can hardly be found in the signal which is less than -30 dB. A similar result is found for CSR, with a small improvement over ISR. However, these results show that sparse regularization can definitely suppress the ambiguity.

Next, we give the results when the non-uniform case is synthesized. The first and second columns in Figure 7 are the results from SR and ISR when the effective aperture interval is 0.04 m. Under this condition, we can see from Figure 7(a) that there are clear artifacts in the SR result which seem like the residue from RCM. This may be caused by the dispersion of the error from the spectrum reconstruction

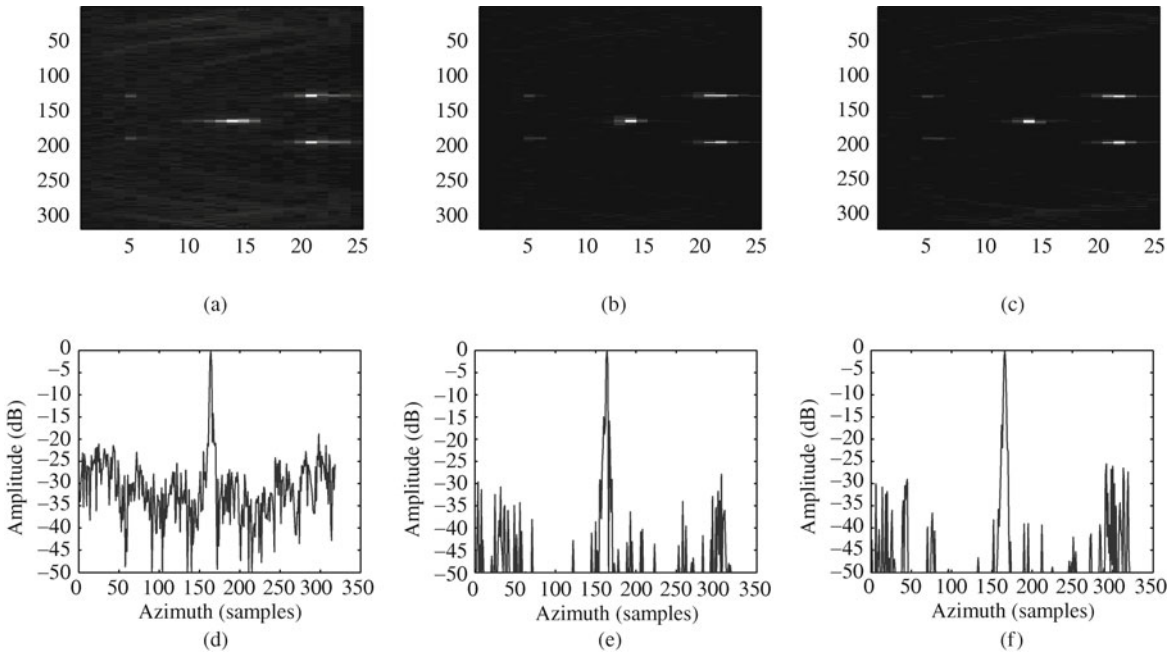

Figure 7 Reconstruction of ground-based data in non-uniform case. (a) 2D result of SR (0.04 m); (b) 2D result of ISR (0.04 m); (c) 2D result of ISR (0.024 m); (d) azimuth profile of SR (0.04 m); (e) azimuth profile of ISR (0.04 m); (f) azimuth profile of ISR (0.024 m).

procedure to the RCMC procedure. However, when using an iterative scheme, the error is iteratively balanced between the two procedures, resulting in a much more robust image. As shown in Figure 7(e), the ambiguity energy is only −28 dB but that of SR is almost −18 dB. Compared with the uniform case, we see a more rapid performance decline in SR than in ISR. We even tested the extreme case where the samples coincide with each other when the effective aperture interval is 0.024 m. SR cannot deal with this situation, because the inverse is undefined. However, as seen in Figure 7(f), the proposed method can still reconstruct the image with an ambiguity level only −25 dB. All of these results show that the proposed method is both robust and effective.

6 Conclusions

In this paper, we have proposed a novel DPCA SAR imaging framework which allows unambiguous wide swath imaging to be performed efficiently and robustly. The main contribution is the strategy to reconstruct the spectrum using sparse regularization, which can maintain the efficiency of the frequency domain methods while avoiding the calculation of the inverse, which is not robust in some cases.

The most important feature is the integration of sparse regularization and the spectrum analysis of the DPCA SAR system. In particular, we modeled the echoes from each sub-receiver in a linear system and combined them into a regularization problem. By using approximation of the DPCA observation with a series of decoupled operators, the proposed method reduces the computational cost from $O(N^2)$ to $O(N \log N)$, when compared with the time domain method. Also, the L_1 sparse regularization scheme is used, which can naturally crack RCM and retrieve the spectrum alternately during the iterations. This leads to the high robustness of the algorithm.

We have applied the algorithm in a series of simulations and problems. The experiments have shown that the proposed method can work under various conditions unambiguously. The key advantage is that the proposed method is more robust than the traditional spectrum reconstruction methods and faster than time-domain methods.

We will further evaluate this method in some practical systems and extend it into a fully compressed sensing framework. With multiple receivers, it is more flexible for design of the sampling strategy, yielding

a CS based wide-swath SAR scheme. The method can also be extended to a multi-input multi-output (MIMO) system to perform more complicated operations.

Acknowledgements

This work was supported by State Key Development Program for Basic Research of China (973) (Grant No. 2010CB731905), Key Program of the National Natural Science Foundation of China (Grant No. 11131006), and National Natural Science Foundations of China (Grant Nos. 61075054, 60975036, and 11171272).

References

1 Currie A, Brown M A. Wide-swath SAR. IEE Proc Radar Sonar Nav, 1992, 139: 122–135
2 Carrara W, Goodman R, Majewski R. Spotlight Synthetic Aperture Radar: Signal Processing Algorithm. Boston: Artech House, 1995
3 Tomiyasu K. Conceptual performance of a satellite borne, wide swath synthetic aperture radar. IEEE Trans Geosci Rem Sens, 1981, 19: 108–116
4 De Zan F, Guarnieri A M. TOPSAR: Terrain observation by progressive scans. IEEE Trans Geosci Rem Sens, 2006, 44: 2352–2360
5 Jean B R, Rouse J W. A multiple beam synthetic aperture radar design concept for geoscience applications. IEEE Trans Geosci Rem Sens, 1983, 21: 201–207
6 Younis M, Fischer C, Wiesbech W. Digital beamforming in SAR systems. IEEE Trans Geosci Rem Sens, 2003, 41: 1735–1739
7 Callaghan G D, Longstaff I D. Wide swath spaceborne SAR using a quad element array. IEE Proc Radar Sonar Nav, 1999, 146: 159–165
8 Suess M, Grafmuller B, Zahn R. A novel high resolution, wide swath SAR system. In: Proceeding of Geoscience and Remote Sensing Symposium, Sydney, 2001
9 Krieger G, Gebert N, Moreira A. Multidimensional waveform encoding: a new digital beamforming technique for synthetic aperture radar remote sensing. IEEE Trans Geosci Rem Sens, 2008, 46: 31–46
10 Gebert N, Krieger G, Moreira A. Unambiguous SAR signal reconstruction from nonuniform displaced phase center sampling. IEEE Trans Geosci Rem Sens Lett, 2004, 1: 260–264
11 Lin Y, Zhang B, Hong W, et al. Displaced phase center antenna SAR imaging based on compressed sensing. In: Proceeding of Geoscience and Remote Sensing Symposium, 2011. 2692–2695
12 Cumming I G, Wong F H. Digital processing of synthetic aperture radar data:algorithms and implementation. Norwood: Artech House, 2005
13 Donoho D L. Compressed sensing. IEEE Trans Inform Theory, 2006, 52: 1289–1306
14 Cetin M, Karl W C. Feature-enhanced synthetic aperture radar image formation based on nonquadratic regularization. IEEE Trans Imag Process, 2001, 10: 623–631
15 Xu Z B. Data modeling: Visual psychology approach and $L_{1/2}$ regularization theory. Proc Int Congr Math, 2010, 4: 3153–3184
16 Daubechies M D I, Mol C D. An iterative thresholding algorithm for linear inverse problems with a sparsity constraint. Commun Pure Appl Math, 2004, 57: 1413–1457
17 Zeng J S, Xu Z B, Jiang H, et al. SAR imaging from compressed measurements based on $L_{1/2}$ regularization. In: Proceeding of Geoscience and Remote Sensing Symposium, Vancouver, 2011. 625–628